INORGANIC CHEMISTRY FRONTIERS

RESEARCH ARTICLE

View Article Online
View Journal | View Issue

Cite this: *Inorg. Chem. Front.*, 2023, **10**, 3706

A PN(Pz)P ligand protected Au_2Cu_2 complex for photoluminescent ultra-low humidity detection with reversible single-crystal-to-single-crystal transformations†

Shengnan Hu,[a] Sisi Yan,[a] Yuanyuan Hu,[a] David James Young,[b] Hong-Xi Li,[a] Chengrong Lu,*[a] Jing-Hui He *[a] and Zhi-Gang Ren *[a]

Received 24th March 2023,
Accepted 16th May 2023

DOI: 10.1039/d3qi00549f

rsc.li/frontiers-inorganic

Reliable and sensitive detection of sub-ppm level, ultra-low humidity is critical for a number of important technologies. We herein report the reaction of a P/N hybrid ligand 3-dppmapz-1-ol with Au(I) and Cu(I) salts resulting in a heteronuclear Au_2Cu_2 cluster complex $[Au_2Cu_2(3\text{-dppmapz})_2](PF_6)_2\cdot 4MeOH$ (**1**·4MeOH) that undergoes reversible single-crystal-to-single-crystal (SCSC) transformations into analogues **1** and **1**·$2H_2O$. The photoluminescent emission of **1**·$2H_2O$ at 625 nm shifted to 617 nm within 24 h and 622 nm after 65 h in P_2O_5 dried air, and returned to green in MeOH/H_2O or MeOH/EtOH vapour. Crystals of **1** could rapidly detect ultralow humidity of 0.21 ppm (w/w).

Introduction

Reliable and sensitive detection of ultra-low humidity is critical for many processes, during which the moisture content needs to be strictly monitored and/or controlled, for example under 500 ppm in microelectronic packaging,[1] 55 ppm in the aviation industry,[2] 10 ppm during reactions involving Grignard and organolithium reagents,[3] and 0.1 ppm in lithium-ion battery manufacturing.[4] Current technology shows good sensitivity in the detection of ultra-low humidity. The most common capacitive sensors consisting of aluminum oxide (γ-Al_2O_3) nanoporous films have achieved a humidity detection range of 3.7–100 ppm.[5] "Enzyme-like" humidity-sensitive chromic materials have achieved naked-eye humidity detection from 0.01–100 ppm.[4] These methods required external electronic circuits or suffered from irreversibility. It is highly desirable to develop more reversible low humidity sensing materials for these important applications.

In recent years, many photoluminescent Au/Ag/Cu complexes have been employed for the reversible detection of organic vapours such as MeOH,[6–10] MeCN,[11–13] THF,[14,15] DMSO,[16–18] and CH_2Cl_2,[19–22] as well as small inorganic molecules including H_2,[23] O_2,[24–28] CO, NO[29] and H_2O[8,30] with good sensitivity, selectivity, reproducibility and portability. The chromic photoluminescent responses of these complexes are attributed to their weak interactions with target molecules, *via* H-bonding,[31–33] C–H···π[9,34,35] and $\pi\cdots\pi$ interactions,[36–38] molecular deformation or formation/disruption of metal–solvent bonds.[7,39–42] For example, Yam and co-workers have reported that the green emission of the cluster $[Au_{10}\{\mu\text{-}Ph_2PN(\text{–}CH_2\text{-}o\text{-}Py)PPh_2\}_4(\mu_3\text{-}S)_4](PF_6)_2$ shifted to blue and red when exposed to CH_2Cl_2 and MeOH vapours, respectively, due to the changing of crystal forms. This emission shifted to yellow on exposure to trifluoroacetic acid (TFA) vapour due to pyridine nitrogen protonation.[43] Ito *et al.* have reported two gold(I) isocyanide complexes displaying reversible photoluminescence transitions between orange and green when exposed to air or saturated MeOH vapour, attributed to the reversible release or inclusion of MeOH in the crystal lattice.[6] However, the intermolecular weak interactions responsible for these colour changes are challenging to elucidate, rendering the putative sensing mechanism less convincing. One reliable way of understanding the underlying chemistry is to observe the configuration of analyte molecules and the host during single crystal transformation.

In this work, we have prepared a new Au/Cu cluster $[Au_2Cu_2(3\text{-dppmapz})_2](PF_6)_2\cdot 4MeOH$ (**1**·4MeOH, 3-dppmapzH = *N*,*N*-bis((diphenylphosphanyl)methyl)-1*H*-pyrazol-3-amine). **1**·4MeOH undergoes reversible single-crystal-to-single-crystal (SCSC) transformation to analogues **1** and **1**·$2H_2O$ on vacuum treatment or solvent exchange. The three compounds emitted

[a]*Suzhou Key Laboratory of Novel Semiconductor-Optoelectronics Materials and Devices, College of Chemistry, Chemical Engineering and Materials Science, Soochow University, Suzhou 215123, China. E-mail: renzhigang@suda.edu.cn*
[b]*Glasgow College UESTC, University of Electronic Science and Technology of China, Chengdu 611731, China*

†Electronic supplementary information (ESI) available. CCDC 2241691–2241693 for **1**, **1**·$2H_2O$ and **1**·4MeOH. For ESI and crystallographic data in CIF or other electronic format see DOI: https://doi.org/10.1039/d3qi00549f

bright red (625 nm, **1**), orange (600 nm, **1**·2H_2O) and green (560 nm, **1**·4MeOH) phosphorescent emissions. The reversible colour change on the formation of **1**·2H_2O was suitable for visible detection of ultra-low humidity changes down to 0.21 ppm (w/w, in P_2O_5 dried air). Complex **1**·2H_2O also exhibited a selective response to MeOH in the presence of water or EtOH.

Results and discussion

The starting ligand 3-dppmapz-1-ol (3-(bis(((diphenylphosphanyl)methyl)amino)-1*H*-pyrazol-1-yl)methanol) was synthesized *via* the Mannich reaction of $HPPh_2$, 3-aminopyrazole and paraformaldehyde in refluxing methanol in a yield of 82% (Scheme S1†). The reaction of 3-dppmapz-1-ol, AuCN, Cu(MeCN)$_4BF_4$ and Et_4NPF_6 in MeOH/CH_2Cl_2 at ambient temperature followed by slow diffusion with hexane produced complex **1**·4MeOH as yellow crystals (Fig. 1). 3-DppmapzH could not be synthesized directly, but was formed *in situ* and deprotonated during this reaction. It seems probable that the Au(I) and Ag(I) salts catalyzed the decomposition of the N–C bond. The PF_6^- counter anion was introduced by the addition of Et_4NPF_6. Attempts using Cu(MeCN)$_4PF_6$ instead of Cu(MeCN)$_4BF_4$ produced uncharacterized white precipitates.

3-Dppmapz-1-ol was insoluble in water, but readily soluble in CH_2Cl_2 and MeOH. The ^{1}H NMR spectrum (Fig. S1†) of 3-dppmapz-1-ol in DMSO-d_6 contained signals for the –CH_2– group (4.14, 5.16 ppm), –OH– group (6.46 ppm), –Ph (7.37–7.33 ppm) and pyrazol group (5.70, 7.50 ppm). One signal for –PPh_2 (−24.75 ppm) was also identified in the ^{31}P{^{1}H} NMR spectrum (Fig. S3†). **1**·2H_2O and **1**·4MeOH were insoluble in water and nonpolar solvent Et_2O, slightly soluble in CH_2Cl_2 and DMSO. The IR spectra of 3-dppmapz-1-ol, **1**·2H_2O and **1**·4MeOH (Fig. S4†) showed signals attributable to the stretching vibrations of –C=N– at 1432, 1433 and 1435 cm^{-1}, respectively. The IR spectra of 3-dppmapz-1-ol and **1**·4MeOH (Fig. S4†) showed stretching vibrations at 1045 and 1027 cm^{-1} attributable to the stretching vibrations of –C–OH. The vibrations at 849 and 847 cm^{-1} were attributable to PF_6^- in **1**·2H_2O and **1**·4MeOH.

The crystal structure of **1**·4MeOH (Fig. 1) at 120 K indicated a square planar tetranuclear Au_2Cu_2 cluster, in which the Au1–Cu1 (2.8227(5) Å), Au1–Cu1A (2.8726(5) Å) and Cu1–Cu1A (2.6723(10) Å) distances are appropriate for metal–metal interactions. The Au1 atom was further coordinated with two P atoms from different dppmapz$^-$ anions with a P1–Au1–P2A angle of 168.48(3)°, while Cu1 was coordinated by two N atoms vertical to the Au_2Cu_2 plane. Two weak Cu···F interactions were also observed in the Au_2Cu_2 plane.

The MeOH molecules in **1**·4MeOH were readily replaced by H_2O in air or liquid water, transforming this complex into analogue **1**·2H_2O (Fig. 2). This transition was reversible. Exposure of **1**·2H_2O crystals to saturated MeOH vapour or immersion in MeOH for several hours gave **1**·4MeOH. The thermogravimetric analysis (TGA, Fig. S5†) curve of **1**·2H_2O indicated the loss of the two water molecules (2.0% w/w) below 110 °C, and indeed this complex gave anhydrous **1** under vacuum (2 h at 100 °C or 24 h at ambient temperature). Likewise, crystals of **1**·4MeOH under vacuum at room temperature produced **1** within 1 h. The PXRD patterns (Fig. 2) of **1**, **1**·2H_2O and **1**·4MeOH matched those simulated from the single-crystal X-ray crystal diffraction (SCXRD) data. Peaks corresponding to **1**·2H_2O appeared in the PXRD spectra of **1** and **1**·4MeOH on exposure to air for 5 min and 10 min, respectively, and these patterns changed completely to that of **1**·2H_2O upon immersion in water within 5 and 30 min, respectively. By comparison, the reverse transformation of **1**·2H_2O to **1**·4MeOH required long-term (12 h) immersion of **1**·2H_2O crystals in liquid MeOH.

Upon excitation at 280–400 nm, crystals of **1**, **1**·2H_2O and **1**·4MeOH emitted brightly at 560 nm (**1**·4MeOH), 600 nm (**1**·2H_2O) and 625 nm (**1**), respectively (Fig. 3a). At room temperature, the emissions were excitation-independent and changing the excitation wavelength from 340 nm to 365 nm did not change the shapes of the emission spectra. The maximum quantum yields (QY) were 0.71 for **1**·2H_2O (λ_{ex} = 365 nm) and 0.80 for 1·4MeOH (λ_{ex} = 350 nm) (the QY of **1** required

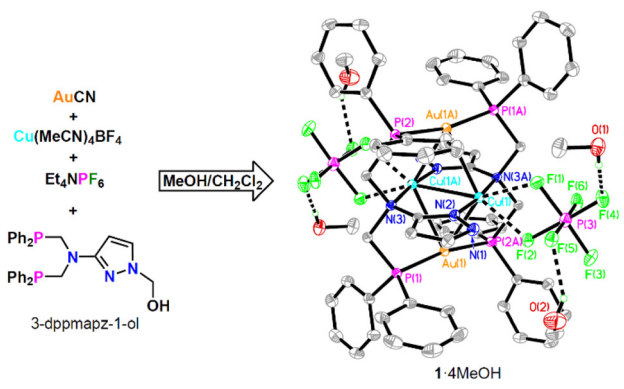

Fig. 1 Synthesis and crystal structure of **1**·4MeOH with 50% thermal ellipsoids. All H atoms except for those of the H-bonded O–H groups are omitted for clarity. Symmetry codes for A: 1 – *x*, 1 – *y*, 1 – *z*; B: 1 – *x*, –*y*, 1 – *z*.

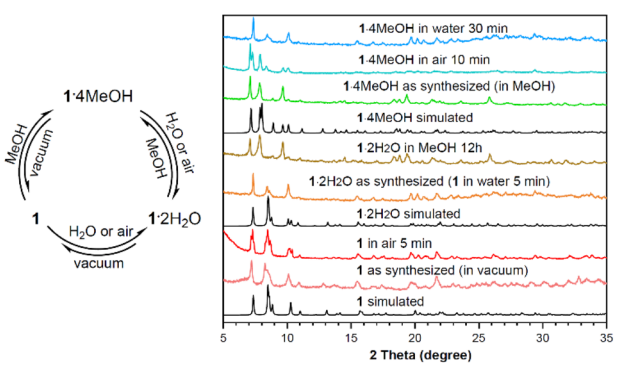

Fig. 2 Reversible inter-conversions of **1**, **1**·2H_2O and **1**·4MeOH, with PXRD patterns simulated from the SCXRD data and those of the samples during the inter-transformations.

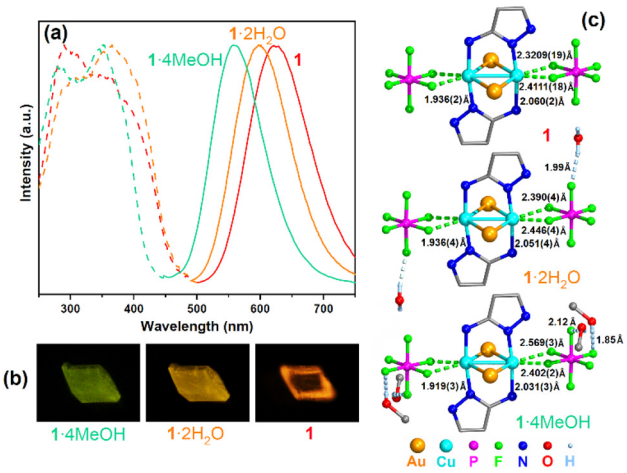

Fig. 3 (a) Excitation (dashed lines) and emission (solid lines) spectra of **1** (red), **1**·2H_2O (orange) and **1**·4MeOH (green) in the solid state. (b) Photos of a single crystal transitioning between the three forms excited under a 365 nm LED light. (c) Central structures of **1**, **1**·2H_2O and **1**·4MeOH, and the distances of the Cu–N bonds, the Cu···F interactions and O–H···F hydrogen bonds from their SCXRD data. All $-CH_2Ph$ groups and H atoms except for O–H are omitted for clarity.

measurement under vacuum and was not acquired), while the lifetimes (τ, excited at 375 nm) were 90.5 μs (**1**), 88.9 μs (**1**·2H_2O) and 94.8 μs (**1**·4MeOH). These relatively long lifetimes and large Stokes shifts (>220 nm) suggested that this photoluminescence was due to phosphorescence emission in each case. The long-term phosphorescence was likely caused by the radiative decay pathway that is formally symmetry-forbidden. Some or all of the relaxation pathways from the locally excited state to the emissive state might involve multiple intermediate electronic states of different symmetries, which could be formally forbidden and thus occur on the long timescale.[44]

The abovementioned interconversions between the three analogues could be demonstrated repeatedly using one single crystal. The emission colour of this crystal changed reversibly (Fig. 3b). The SCXRD measurements at 120 K indicated that the structures of **1** and **1**·2H_2O were similar to that of **1**·4MeOH, except for the distance and orientation of the O–H···F hydrogen bonds between the PF_6^- anions and the H_2O/MeOH molecules. As listed in Table S1,† although all three complexes crystallized in the triclinic crystal system with the $P\bar{1}$ space group, the cell angle of **1** was different from those of **1**·2H_2O and 1·4MeOH. The cell volume of **1** expanded from 1465 $Å^3$ to 1490 $Å^3$ (**1**·2H_2O) and 1629 $Å^3$ (**1**·4MeOH) when the water and MeOH molecules were introduced. Moreover, the PXRD patterns simulated from the SCXRD data were obviously different and indicated phase transitions during the single-crystal-to-single-crystal (SCSC) transformations. Mechanical forces could not lead to such phase transitions as grinding the crystals of **1**·2H_2O didn't cause any emission shift (Fig. S6†).

The photoluminescence of Cu–N complexes is usually attributed to metal-to-ligand charge transfer (MLCT) and thermally activated delayed fluorescence (TADF).[45] Temperature dependent experiments demonstrated that the emissions of **1**, **1**·2H_2O and **1**·4MeOH were blue-shifted when the temperature was gradually decreased from 280 to 80 K (Fig. S7–S9†), while the lifetimes τ shortened slightly (**1**: 87.4 μs; **1**·2H_2O: 73.5 μs; **1**·4MeOH: 74.8 μs), which excludes the possibility of TADF. We subsequently investigated the relationship between solid-state structures and emission. As marked in Fig. 3c, the solid-state structure of **1** contained no hydrogen bonds, but the strongest Cu···F interactions. **1**·2H_2O and **1**·4MeOH possessed more and stronger O–H···F hydrogen bonds and weaker Cu···F interactions. Consequently, the Cu–N bond lengths were commensurately decreased. We speculate that the O–H···F hydrogen bonds between the MeOH and H_2O molecules and the PF_6^- anions attract the electrons of the PF_6^- anions, and therefore weakened the Cu···F interactions, and further strengthened the Cu–N bonds, influencing the energy levels of the ground and excited states of these complexes and blue-shifting the emissions of **1**·2H_2O and **1**·4MeOH.[46]

We performed density functional theory (DFT) and time-dependent DFT (TD-DFT) calculations using the CP2K program[47] and analyzed using the Multiwfn program.[48] The excitation of **1**, **1**·2H_2O and **1**·4MeOH was mainly from the highest occupied molecular orbitals (HOMOs) to the lowest unoccupied molecular orbitals (LUMOs). As shown in Fig. 4 and Fig. S10,† the HOMOs were located at the d orbitals of the Cu atoms (along the Cu–N bonds), while the LUMOs were mainly located at the σ* orbitals of the Au–P bonds, which suggested that the excitation was metal to metal–ligand charge transfer (MMLCT). The energy differences $\Delta E(T_1–S_0)$ between the triplet excited state (T_1) and the singlet ground state (S_0) were 3.02 eV (**1**), 3.06 eV (**1**·2H_2O) and 3.12 eV (**1**·4MeOH), respectively, which were in line with the emission energies of the three compounds.

Exploiting the reversible adsorption and desorption of water molecules, **1**·2H_2O was employed as a photoluminescence probe for the detection of humidity in air and organic solvents. The distinguishable emission shifts were visible to the naked eye when a crystal of **1**·2H_2O transformed into an analogue (Fig. 3b). At room temperature, when **1**·2H_2O (2 mg) was ground and placed in a 100 mL sealed container filled with different desiccants (1 g) for 24 h, its emission (excited at 340 nm, Fig. 5a) was red-shifted to 613, 614, and

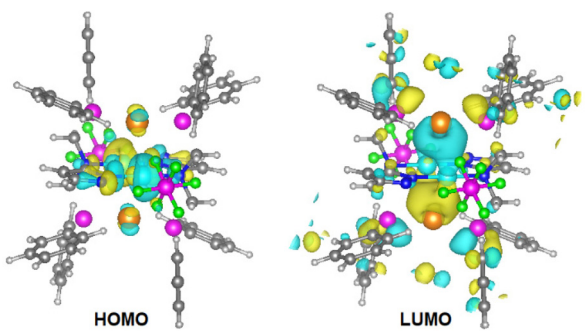

Fig. 4 The distribution of the HOMO and LUMO in **1**.

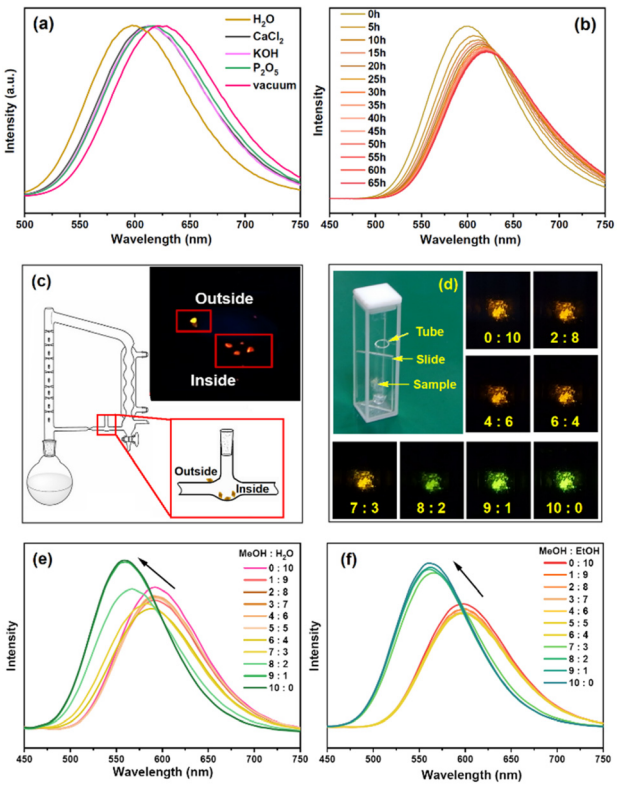

Fig. 5 Emission spectra of **1**·2H_2O (a) in air dried by different desiccants after 24 h, and (b) in air dried by P_2O_5 after different times upon 340 nm excitation. (c) Diagram of the crystals inside and outside of the pipe wall of the return line of an Et_2O reflux equipment. Inset is a photo of the emissions of these crystals (under 365 nm LED) after several hours of reflux. (d) Photos of the equipment used to sense MeOH vapour from MeOH/H_2O and MeOH/EtOH mixtures, and the emissions of **1**·2H_2O in the presence of different molar ratios of MeOH/H_2O under 365 nm LED. (e) and (f) Emission spectra of **1**·2H_2O in the presence of different ratios of MeOH/H_2O and MeOH/EtOH under 360 nm excitation.

617 nm for $CaCl_2$, KOH,[49] and P_2O_5,[50] respectively, which correlated to a water content of 304, 17 and 0.021 ppm (w/w). These emissions were red-shifted by 12 nm ($CaCl_2$ and KOH) and 8 nm (P_2O_5) compared to that of anhydrous **1** (in a vacuum), indicating that **1** was capable of detecting ultra-low humidity changes even in P_2O_5 dried air. This detection limit is comparable to the lowest recorded value of 0.01–100 ppm, determined using nitro-oxazolidine as the sensory material,[4] and is lower than those of other reported optical sensory materials,[51,52] including 1 ppm for SrF_2:Eu^{3+}@TTA nanoparticles[53] and 248 ppm (w/w) for perovskite $CH_3NH_3PbBr_3$.[54] The reversibility between **1** and **1**·2H_2O was further verified by alternatively placing **1**·2H_2O in a vacuum and air, over 5 cycles (Fig. S11†). Time dependent emissions of **1**·2H_2O in the P_2O_5 dried air (Fig. 5b) shifted to 617 nm within 25 h, which moved to 620 nm after 40 h, finally reaching 622 nm after 65 h, indicating that the total loss of solvate from **1**·2H_2O was quite slow. However, the emission of anhydrous **1** recovered to that of **1**·2H_2O very quickly (within seconds) when exposed to air which made the kinetic study difficult.

The photoluminescent responses of **1**·2H_2O to other small inorganic and organic solvents were further investigated. NH_3 and trifluoroacetic acid (TFA) vapour caused emission quenching (Fig. S12†), which was irreversible. PXRD patterns of the samples showed the loss of crystallinity (Fig. S13†), which indicated that some chemical reaction occurred between **1**·2H_2O and NH_3 or TFA. Emissions of **1**·2H_2O on immersing in other organic molecules including EtOH, PrOH (propanol), iPrOH (isopropanol), BuOH (butanol), EG (ethyl glycol), CH_2Cl_2, $CHCl_3$, DMSO, DMF, THF, Et_2O, EA (ethyl acetate), *n*-hexane, CH_3CN, acetone and PE (petroleum ether) indicated that the chromic photoluminescence response was highly selective toward MeOH and DMSO (Fig. 6). These emission wavelengths were quite similar to those of **1** (in DMSO) and **1**·2H_2O (in other solvents), suggesting that DMSO might seize the water molecules from **1**·2H_2O, while other organic solvents could not replace water molecules. It is worth noting that, although **1**·2H_2O was slightly soluble in CH_2Cl_2 and DMSO, the solutions in both solvents gave no obvious emission, which was probably due to the relatively low concentrations.

Both **1** and **1**·2H_2O were insoluble in organic solvents such as Et_2O and THF, and so can be employed to monitor the water content in these solvents that have been dried by refluxing with sodium. As shown in Fig. 5c and Fig. S14,† several crystals of **1**·2H_2O were placed inside the pipe wall of the return line, which emitted red light under a 365 nm LED after refluxing for several hours, while another crystal placed outside still emitted orange. Compared to the traditional indicator benzophenone, **1**·2H_2O has the advantages of rapid sensing, lower dosage, recycling and easy operation with no need for adding a contaminant into the refluxing flask.

Moreover, **1**·2H_2O could also selectively detect MeOH in the presence of H_2O and EtOH. Powdered samples of **1**·2H_2O were coated on quartz slides and each slide was sealed in a quartz cell opening into a small tube containing different ratios of MeOH/H_2O and MeOH/EtOH at room temperature (Fig. 5d). The emission spectra after 10 min indicated obvious changes

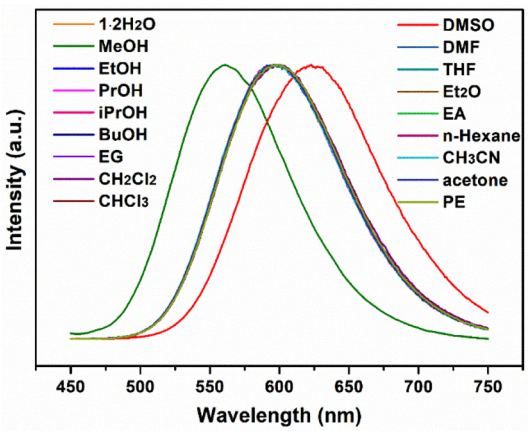

Fig. 6 Emission spectra of **1** 2H_2O on exposure to MeOH, EtOH, PrOH, iPrOH, BuOH, EG, CH_2Cl_2, $CHCl_3$, DMSO, DMF, THF, Et_2O, EA, *n*-hexane, CH_3CN, acetone and PE under 340 nm excitation.

when the molar fraction of MeOH was more than 60% in H_2O (Fig. 5e) and 70% in EtOH (Fig. 5f). The colour change was visible to the naked eye when the molar fraction of MeOH was more than 70% in H_2O (see photos in Fig. 5d).

Conclusions

In summary, **1**·2H_2O is a visible photoluminescent sensor for ultra-low humidity detection. The emissions of **1**, **1**·2H_2O and **1**·4MeOH changed from red to green during their reversible SCSC transformations. This solvent induced photoluminescence chromism can be attributed to changes in O–H···F hydrogen bonding between the solvate molecule and PF_6^-, which influences the Cu···F and Cu–N bond strengths. The photoluminescent chromic response to the transition from **1** to **1**·2H_2O in P_2O_5 dried air (H_2O: 0.021 ppm) is currently the best reversible chemical sensor for humidity detection with potential applications in a number of important technologies.

Experimental section

Materials and methods

Elemental (C, H, and N) analyses (EA) were measured on a Carlo-Erba CHNO-S microanalyzer. Powder X-ray diffraction (PXRD) measurements were recorded on a Panalytical X'Pert-Pro MPD X-ray diffractometer with a Cu Kα source (30 kV, 10 mA) and vacuum equipment. IR spectra were obtained on a VERTEX 70 FT-IR spectrometer (4000–500 cm^{-1}) with an ATR probe. NMR spectra were measured at ambient temperature on a Varian UNITY plus-400 spectrometer, with chemical shifts (δ, ppm) referenced to the solvent signal of DMSO-d_6. Emission spectra, transient photoluminescence and quantum yield measurements were performed on a FLS1000 spectrometer (Edinburgh Instruments, U.K.). Photoluminescence spectra at low temperatures were recorded using an Optistat DN cryostat. Thermogravimetric analysis (TGA) was performed on a SDT2960 analyzer under a N_2 atmosphere and in the temperature range from room temperature to 800 °C, at a heating rate of 10 °C min^{-1}.

Synthesis of 3-dppmapz-1-ol

A mixture of $HPPh_2$ (1.86 g, 10 mmol), 3-aminopyrazole (0.42 g, 5 mmol) and solid paraformaldehyde (0.55 g, 18 mmol) in MeOH (50 mL) was refluxed for 24 h under nitrogen, while the reaction progress was monitored by TLC. The solvent was removed by rotary evaporation and the resulting pale yellow oily crude product was recrystallized from dichloromethane and ethyl ether to give a white solid of 3-dppmapz-1-ol. Yield: 2.09 g (82%). Anal. calcd for $C_{30}H_{29}N_3OP_2$: C, 70.72; H, 5.74; N, 8.25. Found: C, 70.47; H, 5.88; N, 8.18. IR (ATR): 3114 (w), 1555 (s), 1507. (w), 1480 (w), 1430 (m), 1382 (w), 1295 (w), 1263 (m), 1249 (m), 1150 (w), 1056 (s), 989(w), 946(w), 865(w), 836(m), 741(s), 723(m), 695(s), 624(w) cm^{-1}. ^{1}H NMR (400 MHz, DMSO-d_6, ppm) δ 7.50 (d, J = 2.4 Hz, 1H), 7.37–7.33 (m, 20H), 6.46 (t, J = 7.4 Hz, 1H), 5.70 (d, J = 2.4 Hz, 1H), 5.16 (d, J = 7.3 Hz, 2H), 4.14 (s, 4H). ^{13}C NMR (101 MHz, DMSO-d_6, ppm) δ 161.31, 137.93 (d, J = 14.6 Hz), 133.46–133.10 (m), 131.47, 129.21 (d, J = 4.2 Hz), 129.14–128.90 (m), 92.01, 72.83, 52.41. ^{31}P NMR (162 MHz, DMSO-d_6, ppm) δ −24.75.

Synthesis of $[Au_2Cu_2(3\text{-dppmapz})_2](PF_6)_2$·4MeOH (1·4MeOH), 1·2$H_2O$ and 1

A mixture of 3-dppmapz-1-ol (19.2 mg, 0.038 mmol) and AuCN (5.6 mg, 0.025 mmol) in CH_2Cl_2 (1 mL) and MeOH (2 mL) was stirred for 1 h at room temperature to afford a clarified solution. $Cu(MeCN)_4BF_4$ (12.0 mg, 0.038 mmol) and Et_4NPF_6 (3.3 mg, 0.012 mmol) were then added and stirred for 3 h to obtain a yellow turbid solution. The mixture was then centrifuged and the supernatant was slowly diffused with hexane, which afforded light yellow blocks of **1**·4MeOH after 10 days. Yield: 1.4 mg (6.2% based on AuCN). IR (ATR): 3541(w), 3454 (m), 3171(w), 2932(m), 2827(w), 1550(w), 1572(m), 1437(s), 1373(m), 1331(s), 1205(m), 1100(s), 1029(s), 997(m), 896(m), 847(w), 798(m), 700(s), 629(w) cm^{-1}.

1·2H_2O was prepared by immersing **1**·4MeOH in water for 24 h, while **1** was prepared from **1**·4MeOH under vacuum generated by an oil pump (Preiffer Duo 3), at 100 °C for 2 h or at room temperature for 24 h. The yield was quantitative. **1**·2H_2O Anal. calcd for $C_{58}H_{56}Au_2Cu_2F_{12}N_6O_2P_6$: C, 38.62; H, 3.13; N, 4.66. Found: C, 39.46; H, 2.95; N, 5.52. IR (ATR): 3627(w), 3117(w), 3061(w), 2920(w), 1678(w), 1641(w), 1563(w), 1488(w), 1433(m), 1385(w), 1205(w), 1095(m), 999(m), 903(m), 849(w), 798(m), 735(s), 690(s), 634(m).

Single-crystal X-ray structure determinations

Single-crystal X-ray diffraction (SCXRD) data for all crystals were recorded on a Bruker D8 VENTURE diffractometer using Ga Kα radiation (1.34138 Å). Single crystals of **1**·2H_2O and **1**·4MeOH were coated with Paratone oil on a Cryoloop pin, while **1** was sealed in a vacuum capillary tube. An Oxford Cryosystems cryostream at 120 K was used during data collection. Data were processed using the Bruker APEX2 software package using SAINT v8.34A and corrected for absorption by multi-scan. The structures were solved by direct methods and refined on F^2 by full-matrix least-squares using the SHELXTL-2016 program package.[55] All non-hydrogen atoms were refined anisotropically. H atoms of the water molecule in **1**·2H_2O were first located from the difference Fourier maps and then their thermal parameters were constrained to U_{iso}(H) = 1.5U_{eq}(O). All other hydrogen atoms were added theoretically. Selected crystallographic data and refinement parameters are listed in Table S1.†

Conflicts of interest

There are no conflicts to declare.

Acknowledgements

This work was financially supported by the Suzhou Science and Technology Plan Project (Grant No. SGC2021016) and the National Natural Science Foundation of China (Grant No. 21671144).

References

1 Y. Zhang, J. Ren, Y. Wu, X. Zhong, T. Luo, J. Cao, M. Yin, M. Huang and Z. Zhang, Application of moisture-induced discolouration material Nickel(II) iodide in humidity detection, *Sens. Actuators, B*, 2020, **309**, 127769.

2 S. Baena-Zambrana, S. L. Repetto, C. P. Lawson and J. K. W. Lam, Behaviour of water in jet fuel—A literature review, *Prog. Aerosp. Sci.*, 2013, **60**, 35–44.

3 S. Yagi, A. Tanaka, Y. Ichikawa, T. Ichitsubo and E. Matsubara, Effects of water content on magnesium deposition from a Grignard reagent-based tetrahydrofuran electrolyte, *Res. Chem. Intermed.*, 2014, **40**, 3–9.

4 X. Wei, S. X. Zhang and L. Sheng, "Enzyme-Like" Spatially Fixed Polyhydroxyl Microenvironment-Activated Hydrochromic Molecular Switching for Naked Eye Detection of ppm Level Humidity, *Adv. Mater.*, 2023, **35**, 2208261.

5 T. Islam, A. U. Khan, J. Akhtar and M. Z. U. Rahman, A Digital Hygrometer for Trace Moisture Measurement, *IEEE Trans. Ind. Electron.*, 2014, **61**, 5599–5605.

6 M. Jin, T. Sumitani, H. Sato, T. Seki and H. Ito, Mechanical-Stimulation-Triggered and Solvent-Vapor-Induced Reverse Single-Crystal-to-Single-Crystal Phase Transitions with Alterations of the Luminescence Colour, *J. Am. Chem. Soc.*, 2018, **140**, 2875–2879.

7 Z. Lei, S. S. Chang and Q. M. Wang, Vapochromic Gold(I)–Silver(I) Cluster Protected by Alkynyl and Phosphine Ligands, *Eur. J. Inorg. Chem.*, 2017, **2017**, 5098–5102.

8 C. E. Strasser and V. J. Catalano, "On–Off" Au(I)···Cu(I) Interactions in a $Au(NHC)_2$ Luminescent Vapochromic Sensor, *J. Am. Chem. Soc.*, 2010, **132**, 10009–10011.

9 Y. Tao, Y. Wang, S. Hu, D. J. Young, C. Lu, H. X. Li and Z. G. Ren, A photoluminescent Au(I)/Ag(I)/PNN coordination complex for relatively rapid and reversible alcohol sensing, *Dalton Trans.*, 2021, **50**, 6773–6777.

10 S. Wang, Q. Li, S. Yang, H. Yu, J. Chai and M. Zhu, H-bond-induced luminescence enhancement in a Pt_1Ag_{30} nanocluster and its application in methanol detection, *Nanoscale*, 2022, **14**, 16647–16654.

11 Q. Huang, R. Zhang, L. H. He, J. L. Chen, F. Zhao, S. J. Liu and H. R. Wen, Thermo-, Mechano-, and Vapochromic Dinuclear Cuprous-Emissive Complexes with a Switchable CH_3CN-Cu Bond, *Inorg. Chem.*, 2022, **61**, 15629–15637.

12 L. Q. Mo, J. H. Jia, L. J. Sun and Q. M. Wang, Solvent-induced intercluster rearrangements and the reversible luminescence responses in sulfide bridged gold(I)-silver(I) clusters, *Chem. Commun.*, 2012, **48**, 8691–8693.

13 J. Quan, Z.-H. Chen, X. Zhang, J.-Y. Wang, L.-Y. Zhang and Z.-N. Chen, Geometrically isomeric Pt_2Ag_2 acetylide complexes of 2,6-bis(diphenylphosphino)pyridine: luminescent and vapochromic properties, *Inorg. Chem. Front.*, 2021, **8**, 2323–2332.

14 Q. Benito, C. M. Balogh, H. El Moll, T. Gacoin, M. Cordier, A. Rakhmatullin, C. Latouche, C. Martineau-Corcos and S. Perruchas, Luminescence Vapochromism of a Dynamic Copper Iodide Mesocate, *Chem*, 2018, **24**, 18868–18872.

15 S. Evariste, A. M. Khalil, S. Kerneis, C. Xu, G. Calvez, K. Costuas and C. Lescop, Luminescent vapochromic single crystal to single crystal transition in one-dimensional coordination polymer featuring the first Cu(i) dimer bridged by an aqua ligand, *Inorg. Chem. Front.*, 2020, **7**, 3402–3411.

16 J. Lefebvre, R. J. Batchelor and D. B. Leznoff, $Cu[Au(CN)_2]_2(DMSO)_2$: Golden Polymorphs That Exhibit Vapochromic Behavior, *J. Am. Chem. Soc.*, 2004, **126**, 16117–16125.

17 J. Lefebvre, P. Tyagi, S. Trudel, V. Pacradouni, C. Kaiser, J. E. Sonier and D. B. Leznoff, Magnetic Frustration and Spin Disorder in Isostructural $M(\mu\text{-}OH_2)_2[Au(CN)_2]_2$ (M = Mn, Fe, Co) Coordination Polymers Containing Double Aqua-Bridged Chains: SQUID and μSR Studies, *Inorg. Chem.*, 2009, **48**, 55–67.

18 M. A. Mansour, W. B. Connick, R. J. Lachicotte, H. J. Gysling and R. Eisenberg, Linear Chain Au(I) Dimer Compounds as Environmental Sensors: A Luminescent Switch for the Detection of Volatile Organic Compounds, *J. Am. Chem. Soc.*, 1998, **120**, 1329–1330.

19 K. R. England, S. H. Lim, L. M. C. Luong, M. M. Olmstead and A. L. Balch, Vapoluminescent Behavior and the Single-Crystal-to-Single-Crystal Transformations of Chloroform Solvates of $[Au_2$(mu-1,2-bis(diphenylarsino)ethane$)_2$ $](AsF_6)_2$, *Chem*, 2019, **25**, 874–878.

20 M. S. Jiang, Y. H. Tao, Y. W. Wang, C. Lu, D. J. Young, J. P. Lang and Z. G. Ren, Reversible Solid-State Phase Transitions between Au-P Complexes Accompanied by Switchable Fluorescence, *Inorg. Chem.*, 2020, **59**, 3072–3078.

21 M. A. Malwitz, S. H. Lim, R. L. White-Morris, D. M. Pham, M. M. Olmstead and A. L. Balch, Crystallization and interconversions of vapor-sensitive, luminescent polymorphs of $[(C_6H_{11}NC)_2Au(I)](AsF_6)$ and $[(C_6H_{11}NC)_2Au(I)](PF_6)$, *J. Am. Chem. Soc.*, 2012, **134**, 10885–10893.

22 T. Seki, M. Jin and H. Ito, Introduction of a Biphenyl Moiety for a Solvent-Responsive Aryl Gold(I) Isocyanide Complex with Mechanical Reactivation, *Inorg. Chem.*, 2016, **55**, 12309–12320.

23 S. Basu, A. Paul and A. Chattopadhyay, Zinc mediated crystalline assembly of gold nanoclusters for expedient hydrogen storage and sensing, *J. Mater. Chem. A*, 2016, **4**, 1218–1223.

24 G. Chakkaradhari, Y. T. Chen, A. J. Karttunen, M. T. Dau, J. Janis, S. P. Tunik, P. T. Chou, M. L. Ho and I. O. Koshevoy, Luminescent Triphosphine Cyanide d^{10} Metal Complexes, *Inorg. Chem.*, 2016, **55**, 2174–2184.

25 R. W. Huang, Y. S. Wei, X. Y. Dong, X. H. Wu, C. X. Du, S. Q. Zang and T. C. W. Mak, Hypersensitive dual-function luminescence switching of a silver-chalcogenolate cluster-based metal-organic framework, *Nat. Chem.*, 2017, **9**, 689–697.

26 E. Khatun, A. Ghosh, P. Chakraborty, P. Singh, M. Bodiuzzaman, P. Ganesan, G. Nataranjan, J. Ghosh, S. K. Pal and T. Pradeep, A thirty-fold photoluminescence enhancement induced by secondary ligands in monolayer protected silver clusters, *Nanoscale*, 2018, **10**, 20033–20042.

27 L.-Y. Yao, K.-H. Low and V. W.-W. Yam, A Gold Quartet Framework with Reversible Anisotropic Structural Transformation Accompanied by Luminescence Response, *Chem*, 2019, **5**, 2418–2428.

28 L. Zhang, F. Lin, M. Ye, D. Tian, J. Jin, Y. Huang, Y. Jiang, Y. Wang and X. Chen, Luminescence sensing of oxygen using copper iodide hybrid material, *Sens. Actuators, B*, 2021, **346**, 130566.

29 Y. Yong, C. Li, X. Li, T. Li, H. Cui and S. Lv, Ag_7Au_6 Cluster as a Potential Gas Sensor for CO, HCN, and NO Detection, *J. Phys. Chem. C*, 2015, **119**, 7534–7540.

30 K. Igawa, N. Yoshinari, M. Okumura, H. Ohtsu, M. Kawano and T. Konno, Crystalline-Amorphous-Crystalline Transformation in a Highly Brilliant Luminescent System with Trigonal-Planar Gold(I) Centers, *Sci. Rep.*, 2016, **6**, 26002.

31 J. Han, S. C. Cheng, S. M. Yiu, M. K. Tse and C. C. Ko, Luminescent monomeric and dimeric Ru(ii) acyclic carbene complexes as selective sensors for NH_3/amine vapor and humidity, *Chem. Sci.*, 2021, **12**, 14103–14110.

32 H. Inoue, Y. Yamashita, Y. Ozawa, T. Ono and M. Abe, Solid-State Structures and Photoluminescence of Lamellar Architectures of Cu(I) and Ag(I) Paddlewheel Clusters with Hydrogen-Bonded Polar Guests, *Molecules*, 2021, **26**, 6731.

33 S. Yokomori, S. Dekura, T. Fujino, M. Kawamura, T. Ozaki and H. Mori, Vapochromism induced by intermolecular electron transfer coupled with hydrogen-bond formation in zinc dithiolene complex, *J. Mater. Chem. C*, 2020, **8**, 14939–14947.

34 Y. Li, S. Zhang and D. Song, A luminescent metal-organic framework as a turn-on sensor for DMF vapor, *Angew. Chem., Int. Ed.*, 2013, **52**, 710–713.

35 D. Qiao, J. Y. Wang, L. Y. Zhang, F. R. Dai and Z. N. Chen, Aggregation-induced emission enhancement and reversible mechanochromic luminescence of quinoline-based zinc(II)-Schiff base complexes, *Dalton Trans.*, 2019, **48**, 11045–11051.

36 Z. M. Hudson, C. Sun, K. J. Harris, B. E. G. Lucier, R. W. Schurko and S. Wang, Probing the Structural Origins of Vapochromism of a Triarylboron-Functionalized Platinum(II) Acetylide by Optical and Multinuclear Solid-State NMR Spectroscopy, *Inorg. Chem.*, 2011, **50**, 3447–3457.

37 B. Jiang, J. Zhang, J.-Q. Ma, W. Zheng, L.-J. Chen, B. Sun, C. Li, B.-W. Hu, H. Tan, X. Li and H.-B. Yang, Vapochromic Behavior of a Chair-Shaped Supramolecular Metallacycle with Ultra-Stability, *J. Am. Chem. Soc.*, 2016, **138**, 738–741.

38 Y. J. Li, Z. Y. Deng, X. F. Xu, H. B. Wu, Z. X. Cao and Q. M. Wang, Methanol triggered ligand flip isomerization in a binuclear copper(I) complex and the luminescence response, *Chem. Commun.*, 2011, **47**, 9179–9181.

39 K. Chen, J. Shearer and V. J. Catalano, Subtle Modulation of $Cu_4X_4L_2$ Phosphine Cluster Cores Leads to Changes in Luminescence, *Inorg. Chem.*, 2015, **54**, 6245–6256.

40 A. Laguna, T. Lasanta, J. M. López-de-Luzuriaga, M. Monge, P. Naumov and M. E. Olmos, Combining Aurophilic Interactions and Halogen Bonding To Control the Luminescence from Bimetallic Gold–Silver Clusters, *J. Am. Chem. Soc.*, 2010, **132**, 456–457.

41 Z. Lei, X. L. Pei, Z. G. Jiang and Q. M. Wang, Cluster linker approach: preparation of a luminescent porous framework with NbO topology by linking silver ions with gold(I) clusters, *Angew. Chem., Int. Ed.*, 2014, **53**, 12771–12775.

42 L.-Y. Zhang, L.-J. Xu, X. Zhang, J.-Y. Wang, J. Li and Z.-N. Chen, Spectroscopic and Phosphorescent Modulation in Triphosphine-Supported $PtAg_2$ Heterotrinuclear Alkynyl Complexes, *Inorg. Chem.*, 2013, **52**, 5167–5175.

43 A. Chu, F. K.-W. Hau, L.-Y. Yao and V. W.-W. Yam, Decanuclear Gold(I) Sulfido Pseudopolymorphs Displaying Stimuli-Responsive RGBY Luminescence Changes, *ACS Mater. Lett.*, 2019, **1**, 277–284.

44 K. Zhang, Y. Shen, X. Yang, J. Liu, T. Jiang, N. Finney, B. Spingler and S. Duttwyler, Atomically Defined Monocarborane Copper(I) Acetylides with Structural and Luminescence Properties Tuned by Ligand Sterics, *Chem. – Eur. J.*, 2019, **25**, 8754–8759.

45 D. Felder, J.-F. Nierengarten, F. Barigelletti, B. Ventura and N. Armaroli, Highly Luminescent Cu(I)–Phenanthroline Complexes in Rigid Matrix and Temperature Dependence of the Photophysical Properties, *J. Am. Chem. Soc.*, 2001, **123**, 6291–6299.

46 B. Hupp, J. Nitsch, T. Schmitt, R. Bertermann, K. Edkins, F. Hirsch, I. Fischer, M. Auth, A. Sperlich and A. Steffen, Stimulus-Triggered Formation of an Anion-Cation Exciplex in Copper(I) Complexes as a Mechanism for Mechanochromic Phosphorescence, *Angew. Chem., Int. Ed.*, 2018, **57**, 13671–13675.

47 T. D. Kuhne, M. Iannuzzi, M. Del Ben, V. V. Rybkin, P. Seewald, F. Stein, T. Laino, R. Z. Khaliullin, O. Schutt, F. Schiffmann, D. Golze, J. Wilhelm, S. Chulkov, M. H. Bani-Hashemian, V. Weber, U. Borstnik, M. Taillefumier, A. S. Jakobovits, A. Lazzaro, H. Pabst, T. Muller, R. Schade, M. Guidon, S. Andermatt, N. Holmberg, G. K. Schenter, A. Hehn, A. Bussy, F. Belleflamme, G. Tabacchi, A. Gloss, M. Lass, I. Bethune, C. J. Mundy, C. Plessl, M. Watkins, J. VandeVondele, M. Krack and J. Hutter, CP2K: An electronic structure and molecular dynamics software package - Quickstep: Efficient and accurate electronic structure calculations, *J. Chem. Phys.*, 2020, **152**, 194103.

48 T. Lu and F. Chen, Multiwfn: a multifunctional wavefunction analyzer, *J. Comput. Chem.*, 2012, **33**, 580–592.

49 G. P. Baxter and H. W. Starkweather, The Efficiency of Calcium Chloride, Soldium Hydroxide and Potassium

Hydroxide as Drying Agents, *J. Am. Chem. Soc.*, 1916, **38**, 2038–2041.
50 E. W. Morley, Note on the Amount of Moisture Remaining in a Gas after Drying with Phosphorus Pentoxide, *J. Am. Chem. Soc.*, 1904, **26**, 1171–1173.
51 Y. Guo and W. Zhao, Nanomaterials for luminescent detection of water and humidity, *Analyst*, 2019, **144**, 388–395.
52 A. Jouyban and E. Rahimpour, Optical sensors for determination of water in the organic solvents: a review, *J. Iran. Chem. Soc.*, 2021, **19**, 1–22.
53 D. Ghosh and M. N. Luwang, One-pot synthesis of 2-thenoyltrifluoroacetone surface functionalised SrF_2:Eu^{3+} nanoparticles: trace level detection of water, *RSC Adv.*, 2015, **5**, 47131–47139.
54 W. Xu, F. Li, Z. Cai, Y. Wang, F. Luo and X. Chen, An ultrasensitive and reversible fluorescence sensor of humidity using perovskite $CH_3NH_3PbBr_3$, *J. Mater. Chem. C*, 2016, **4**, 9651–9655.
55 G. M. Sheldrick. *SHELXTL-2016*, Universität Göttingen, Göttingen Germany, 2016.